

TABLE I. Mo^{5+} $4d$ -shell splittings ($j = 3/2$ to $j = 1/2$ and $t_{2g}-e_g$) and ‘static’ g_{\parallel} factor in cubic Ba_2YMoO_6 . Three orbitals ($4d$ t_{2g}) were active in the CASSCF calculation for $\Delta_{3/2 \rightarrow 1/2}$ while five orbitals were active in the calculations for g_{\parallel} and $\Delta_{t_{2g} \rightarrow e_g}$ (sans SOC for the latter).

$4d^1$ electronic structure	CASSCF	MRCI
$\Delta_{3/2 \rightarrow 1/2}$ (eV)	0.133	0.130
$\Delta_{t_{2g} \rightarrow e_g}$ (eV)	4.80	4.51
g_{\parallel}	0.18	0.20

Here we carry out a detailed *ab initio* investigation of the Mo^{5+} $4d^1$ and Os^{7+} $5d^1$ relativistic electronic structure in the double-perovskite compounds Ba_2YMoO_6 , $\text{Ba}_2\text{LiOsO}_6$ and $\text{Ba}_2\text{NaOsO}_6$. In addition to providing reliable results for the energy scale of the d -level splittings, $t_{2g}-e_g$ and induced by SOC within the t_{2g}^1 manifold, we analyze the role of TM $d-O p$ orbital mixing plus the strength of electron-lattice couplings. It is found that strong metal $d-O p$ hybridization generates a finite magnetic moment even for perfectly cubic environment around the TM site, providing *ab initio* support to the phenomenological covalency factor introduced in this context by Stevens [21]. The TM d^1 magnetic moment is further enhanced by tetragonal distortions, against which the octahedral oxygen cage is unstable. According to our results, such Jahn-Teller (JT) effects are particularly strong for the Mo $4d^1$ ions in Ba_2YMoO_6 . While additional investigations are needed for clarifying the role of intersite cooperative couplings [22, 23], our calculations thus emphasize the high sensitivity of the effective magnetic moments to both metal-ligand covalency effects and local JT physics. The material dependence for the ratio among the strengths of the spin-orbit interaction, the JT coupling parameter and the effective covalency factor that we compute here provide a solid basis for future studies addressing the role of intersite interactions on the double-perovskite *fcc* lattice.

RESULTS

Quantum chemistry calculations were first performed to resolve the essential features of the electronic structure of the cubic lattice configuration, without accounting for electron-lattice couplings (see Methods for computational details and Fig. 1 for a sketch of a three-dimensional double-perovskite crystal). Results for the splitting between the Mo^{5+} t_{2g}^1 $j = 3/2$ and $j = 1/2$ spin-orbit states, $\Delta_{3/2 \rightarrow 1/2}$, are provided in Table I at two levels of approximation, i. e., multiconfiguration complete-active-space self-consistent-field (CASSCF) and multireference configuration-interaction (MRCI) with single and double excitations on top of the CASSCF wave function [24]. Knowing the splitting $\Delta_{3/2 \rightarrow 1/2}$, the strength of the SOC parameter can be easily derived as $\lambda = \frac{2}{3} \Delta_{3/2 \rightarrow 1/2}^{\text{CASSCF}}$ [11]. The resulting λ of 89 meV is somewhat smaller than earlier estimates of 99 meV for Mo^{5+} impurities in SrTiO_3

[25]. A most interesting finding, however, is that despite the cubic environment the quantum chemistry calculations yield a nonvanishing magnetic moment and a finite g factor. This obviously does not fit the nonmagnetic $j = 3/2$ quartet ground state assumed to arise in standard textbooks on crystal-field theory [11, 12] from exact cancellation between the spin and the orbital moments.

At a qualitative level, it has been argued by Stevens [21] that finite g -factor values can in fact occur for $j = 3/2$ ions due to TM-O covalency on the TM O_6 octahedron. For better insight into the nature of such effects we therefore performed a simple numerical experiment in which the six ligands coordinating the reference Mo^{5+} $4d^1$ ion are replaced by -2 point charges with no atomic basis functions. In that additional set of computations the magnetic moment and the g factor do vanish, in agreement with the purely ionic picture of Kotani, Abragam and Bleaney [10, 11]. This shows that one tuning knob for switching magnetism on is indeed the TM $4d-O 2p$ orbital hybridization. The latter is strong for high ionization states such as Mo^{5+} (as the tails of the $4d$ -like valence orbitals indicate in the case the nearest-neighbor ligands are provided with atomic basis sets, see Fig. 2(a), gives rise to partial quenching of the orbital moment and makes that the exact cancellation between the spin and the orbital moments no longer holds.

We find that this effect is even stronger for the formally $7+$ Os ion in $\text{Ba}_2\text{LiOsO}_6$ and $\text{Ba}_2\text{NaOsO}_6$. As shown in Table II, g factors as large as 0.4 are computed in this case. The quantum chemistry results also allow us to estimate the strength of the effective Os^{7+} $5d^1$ SOC constant, with $\lambda = \frac{2}{3} \Delta_{3/2 \rightarrow 1/2}^{\text{CASSCF}} = 387$ meV, lower than $\lambda = 468$ meV in tetravalent $5d^5$ iridates [26].

Since the t_{2g}^1 electron configuration is susceptible to JT effects, we carried out further investigations on the stability of an ideal TM O_6 octahedron against tetragonal (z -axis) distortions. A total-energy profile for specified geometric configurations is provided in Fig. 2(c) for an embedded MoO_6 octahedron. It is seen that the minimum corresponds to about

TABLE II. Os^{7+} $5d$ -shell splittings ($j = 3/2$ to $j = 1/2$ and $t_{2g}-e_g$) and ‘static’ g_{\parallel} factors in cubic $\text{Ba}_2\text{LiOsO}_6$ and $\text{Ba}_2\text{NaOsO}_6$. Only the $5d$ t_{2g} orbitals were active in the CASSCF calculation for $\Delta_{3/2 \rightarrow 1/2}$; all five $5d$ orbitals were active in the calculations for g_{\parallel} and $\Delta_{t_{2g} \rightarrow e_g}$. For the latter, values including SOC are provided within parantheses. All energies in eV.

$5d^1$ electronic structure	CASSCF	MRCI
$\text{Ba}_2\text{LiOsO}_6$:		
$\Delta_{3/2 \rightarrow 1/2}$	0.58	0.56
$\Delta_{t_{2g} \rightarrow e_g}$	6.17 (6.44)	5.95 (6.21)
g_{\parallel}	0.39	0.40
$\text{Ba}_2\text{NaOsO}_6$:		
$\Delta_{3/2 \rightarrow 1/2}$	0.58	0.57
$\Delta_{t_{2g} \rightarrow e_g}$	6.41 (6.68)	6.19 (6.45)
g_{\parallel}	0.31	0.40

3% tetragonal compression, as compared to the cubic octahedron of the $Fm\bar{3}m$ crystalline structure [14]. As expected, the magnetic moment rapidly increases in the presence of distortions, as illustrated in Table III and Fig. 2(d).

Depending on further details related to the strength of the intersite couplings among ‘JT centers’, *static* deformations away from cubic symmetry may be realized in some systems, as observed for example in the $\text{Re}^{6+} 5d^1$ double perovskite $\text{Sr}_2\text{MgReO}_6$ [27] and rare-earth molybdates [28, 29]. If the local JT couplings and intersite interactions are relatively weak, one may be left on the other hand in a *dynamic* JT regime, as earlier pointed out for the particular t_{2g}^1 configuration by, e.g., Kahn and Kettle [30]. The relevant vibrational modes that couple to the ${}^2T_{2g}(t_{2g}^1)$ electronic term are those of E_g symmetry [($3z^2 - r^2$)- and ($x^2 - y^2$)-like]. From the quantum chemistry calculations, we find that the potential-energy well is significantly shallower for these normal coordinates, as compared to z -axis-only compression. The value we computed for the Mo^{5+} ion in Ba_2YMoO_6 , ≈ 40 meV, is comparable to the estimate made in the 1970’s for $\text{Mo}^{5+} t_{2g}^1$ impurity ions within the SrTiO_3 matrix, ≈ 60 meV [25].

For the osmates, the depth of this potential well is much reduced, with E_{JT} values in the range of 10–15 meV by spin-orbit MRCI calculations (see Table IV).

The vibronic model of Kahn and Kettle [30] provides specific expressions for the g factors. In particular, g_{\parallel} can be parametrized as [30]

$$g_{\parallel} = 2(1 - k_{\text{cov}}k_{\text{vib}}), \quad (1)$$

where k_{cov} is Stevens’ covalency factor [21] and

$$k_{\text{vib}} = \exp[-x/(1 + \rho)]. \quad (2)$$

The parameters x and ρ are defined as [30] $x = 3E_{\text{JT}}/2\hbar\omega$ and $\rho = 3\lambda/2\hbar\omega$, where $\hbar\omega$ is the E_g -mode vibrational energy, and $g_{\perp} = 0$ by symmetry [11, 21, 30]. Recent infrared transmission spectra indicate that $\hbar\omega \approx 560 \text{ cm}^{-1} \approx 70$ meV for the bond stretching phonons [17, 31]. The effective parameter k_{cov} we can easily evaluate from the static g_{\parallel} values obtained in the MRCI spin-orbit treatment (see Tables I and II) if vibronic interactions are neglected ($k_{\text{vib}} = 1$ for ‘frozen’ cubic octahedra), with $k_{\text{cov}} \equiv 1 - g_{\parallel}^{\text{MRCI}}/2$. This yields covalency reduction factors of 0.90 for Ba_2YMoO_6 and 0.80 for the osmates.

Estimates for g_{\parallel} are provided in Table IV, using the Kahn-Kettle vibronic model and the quantum chemistry results for λ , k_{cov} and E_{JT} . It is seen that a large ρ/x ratio (i.e., large λ/E_{JT}) makes that g_{\parallel} is generated mostly through covalency effects in the osmates, with minor contributions from vibronic couplings. On the other hand, the small ρ/x ratio in Ba_2YMoO_6 gives rise to a strong enhancement of g_{\parallel} through vibronic effects, with a factor of nearly 4 between $(1 - k_{\text{cov}}k_{\text{vib}})$ and $(1 - k_{\text{cov}})$. This way, the interesting situation arises that the TM magnetic moment is mainly due to vibronic effects in Ba_2YMoO_6 and predominantly to strong covalency in $\text{Ba}_2\text{LiOsO}_6$ and $\text{Ba}_2\text{NaOsO}_6$.

TABLE III. $\text{Mo}^{5+} t_{2g}^1$ electronic structure with ‘static’ tetragonal squeezing of the reference MoO_6 octahedron. Only the t_{2g}^1 configuration was considered in the reference CASSCF. $\Delta_{t_{2g}}$ is t_{2g} tetragonal splitting without SOC, δ_1 and δ_2 are excitation energies within the t_{2g}^1 manifold with SOC accounted for ($\delta_1 = 0$ and $\delta_2 = \Delta_{3/2 \rightarrow 1/2}$ for cubic octahedra, see Fig. 2(b)). MRCI results, all energies in eV.

MoO_6 flattening	0.5%	1.5%	3%	5%
$\Delta_{t_{2g}}$	0.02	0.07	0.15	0.27
δ_1	0.02	0.05	0.12	0.24
δ_2	0.14	0.17	0.23	0.33
μ_{\parallel} (μ_{B})	0.24	0.55	0.75	0.89
g_{\parallel} ($k_{\text{vib}} = 1$)	0.50	1.09	1.55	1.80

DISCUSSION

Experimentally, the measured magnetic moments are indeed significantly smaller in $\text{Ba}_2\text{LiOsO}_6$ and $\text{Ba}_2\text{NaOsO}_6$ [19, 20] as compared to Ba_2YMoO_6 [13, 14, 17, 25]. With regard to the estimates we make here for g_{\parallel} , possible sources of errors concern the accuracy of the calculated E_{JT} when using the experimental crystal structure as reference and correlation and polarisation effects beyond a single TMO_6 octahedron [32, 33]. The latter effects would only increase E_{JT} . With respect to the former aspect, it is known that by advanced quantum chemistry calculations the lattice constants of TM oxides can be computed with deviations of less than 0.5% from the measured values [32], which implies rather small corrections to E_{JT} . Interestingly, recent findings of additional phonon modes at low temperatures [17] indicate static distortions of the MoO_6 octahedra in Ba_2YMoO_6 and indeed a rather large E_{JT} . More detailed investigations on this matter are left for future work. Valuable experimental data that can be directly compared to our calculations would be the results of electron spin resonance measurements of the g factors.

It is also worth pointing out that using the Kahn-Kettle model even a E_{JT} of 75 meV, 5 to 7 times larger than the values computed by MRCI for the osmates (see Table IV), still yields a rather moderate g_{\parallel} factor of 0.65 for the Os $5d^1$ ion. Such g_{\parallel} factors of 0.4–0.6 compare quite well with the low-temperature magnetic moment derived from magnetization and muon spin relaxation measurements on $\text{Ba}_2\text{NaOsO}_6$, $\approx 0.2 \mu_{\text{B}}$ [19, 20]. For the Mo $4d^1$ ion in Ba_2YMoO_6 , the computed g_{\parallel} factor is much more sensitive to variations of E_{JT} — increasing E_{JT} from, e.g., 40 to 200 meV enhances g_{\parallel} of Eq. (1) from ≈ 0.6 to ≈ 1.6 .

One other remarkable prediction of Kahn and Kettle [30] is that the splitting of the $j = 3/2$ and $j = 1/2$ states is increased through vibronic couplings, by a factor

$$\gamma = 1 + x \frac{3 + \rho}{3(\rho^2 - 1)}. \quad (3)$$

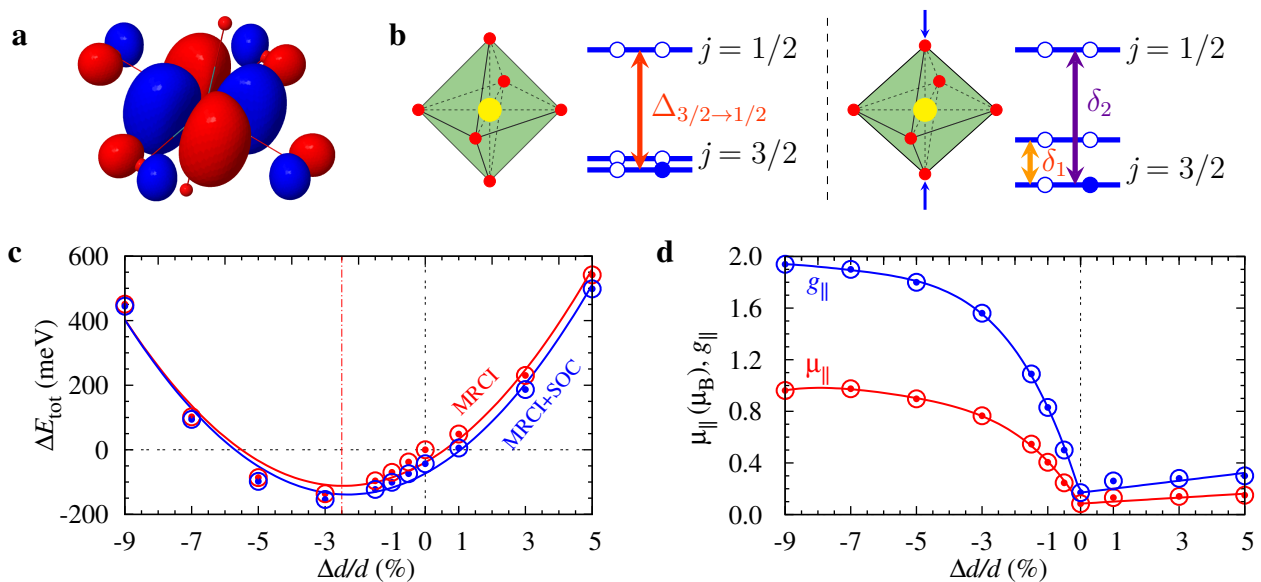


FIG. 2. a) Mo $4d$ t_{2g} charge density as obtained by CASSCF calculations. The tails at the nearest-neighbor O sites have substantial weight. b) TM t_{2g} splittings in cubic (left) and tetragonal (right) symmetry; $\delta_1 = 0$ and $\delta_2 = \Delta_{3/2 \rightarrow 1/2}$ for cubic octahedra. c) Ground-state energy as function of z -axis tetragonal distortion, MRCI results both with and without spin-orbit coupling. d) Variation of the Mo $4d^1$ magnetic moment ($\mu_{||}$) and g factor ($g_{||}$) with the amount of z -axis tetragonal distortion, MRCI results including spin-orbit interactions.

This effect turns out to be small in the osmates, given the small x and large ρ in those compounds. But we compute a strong modification of the $j = 3/2$ to $j = 1/2$ excitation energy for Ba_2YMoO_6 , from about 0.13 eV in the absence of vibronic interactions (see Table I) to ≈ 0.20 eV with Jahn-Teller effects included ($E_{\text{JT}} = 40$ meV). Experimentally the situation can be clarified by direct resonant inelastic x-ray scattering (RIXS) measurements on Ba_2YMoO_6 . High-resolution RIXS measurements could also address the occurrence of static distortions at low temperatures, suggested for Ba_2YMoO_6 on the basis of extra phonon modes in the low- T infrared transmission spectra [17] and for $\text{Ba}_2\text{NaOsO}_6$ from the integrated entropy through the magnetic phase transition at about 7 K [19]. According to the MRCI data in Table III, a reduction by 0.5–1.5% of the interatomic distances on one set of O–Mo–O links already gives a splitting of 20–50 meV of the low-lying spin-orbit states. Splittings of this size should be accessible with last-generation RIXS apparatus.

Also of interest is an experimental confirmation of the un-

usually large t_{2g} – e_g gap we predict in the double-perovskite heptavalent osmates, $\gtrsim 6$ eV (see Table II). According to the results of additional computations we carried out, the source of this exceptional d -level splitting is the stabilization of the Os t_{2g} states due to the large effective charge (formally $7+$) at the nearest-neighbor Os sites. The latter are situated on the axes along which the lobes of the t_{2g} orbitals are oriented; in contrast, the lobes of the e_g functions point towards the monovalent species (Li^{1+} or Na^{1+}). For example, test CASSCF calculations in which the size of the point charges placed at the 12 Os and 6 alkaline-ion nearest-neighbor sites are modified from the formal ionic values $7+$ and $1+$ ($12 \times 7 + 6 \times 1 = 90$) to $5+$ and $5+$ ($12 \times 5 + 6 \times 5 = 90$) show a reduction of about 2 eV of the t_{2g} – e_g level splitting. Similar effects, with relative shifts and even inversion of the d -electron energy levels due to charge imbalance at nearby cation sites, were recently evidenced in Sr_2RhO_4 and Sr_2IrO_4 [8, 26], the rare-earth 227 iridates $R_2\text{Ir}_2\text{O}_7$ [34] and $\text{Cd}_2\text{Os}_2\text{O}_7$ [35]. The mechanism has not been thoroughly explored so far experimentally but seems to hold much potential in the context of orbital engineering in TM compounds.

TABLE IV. TM $g_{||}$ factors using the Kahn-Kettle vibronic model [30] and *ab initio* estimates for λ , k_{cov} and E_{JT} . $x = 3E_{\text{JT}}/2\hbar\omega$, $\rho = 3\lambda/2\hbar\omega$, $\hbar\omega$ is set to 70 meV [17, 31] and $g_{||} = 2(1 - k_{\text{cov}}k_{\text{vib}})$.

	E_{JT}	x	ρ	k_{vib}	k_{cov}	$g_{ }$
$\text{Mo}^{5+} 4d^1$, Ba_2YMoO_6	40	0.86	1.90	0.74	0.90	0.66
$\text{Os}^{7+} 5d^1$, $\text{Ba}_2\text{LiOsO}_6$	10	0.21	8.29	0.98	0.80	0.44
$\text{Os}^{7+} 5d^1$, $\text{Ba}_2\text{NaOsO}_6$	15	0.32	8.29	0.97	0.80	0.45

To summarize, it is well known that nominal orbital degeneracy gives rise in $3d$ transition-metal oxides to subtle couplings between the electronic and lattice degrees of freedom and very rich physics. Here we resolve the effect of electron-lattice interactions on the magnetic properties of heavier, $4d$ and $5d$ transition-metal ions with a formally degenerate t_{2g}^1 electron configuration in the double-perovskite materials Ba_2YMoO_6 , $\text{Ba}_2\text{LiOsO}_6$ and $\text{Ba}_2\text{NaOsO}_6$. In particular, by using advanced quantum

chemistry electronic-structure calculations, we reconcile the notion of a nonmagnetic spin-orbit-coupled t_{2g}^1 , $j = 3/2$ ground state put forward by Kotani, Abragam, Bleaney and others [10–12] with the variety of magnetic properties recently observed in $4d^1$ and $5d^1$ double perovskites. Our analysis shows that the sizable magnetic moments and g factors found experimentally are due to strong TM d -ligand p hybridization and dynamic Jahn-Teller effects, providing new perspectives on the interplay between metal-ligand interactions and spin-orbit couplings in transition-metal oxides. It also highlights the proper theoretical frame for addressing the remarkably rich magnetic properties of d^1 double perovskites [2, 15, 16, 19, 20] in particular. Over the last two decades, vibronic couplings have unjustifiably received low attention in the case of these intriguing materials.

METHODS

All *ab initio* calculations were carried out with the quantum chemistry package MOLPRO [36]. Crystallographic data as derived in Ref. [14] for Ba_2YMoO_6 and in Ref. [18] for $\text{Ba}_2\text{LiOsO}_6$ and $\text{Ba}_2\text{NaOsO}_6$ were employed.

We used effective core potentials (ECP’s), valence basis functions of triple-zeta quality and two f polarization functions for the reference Mo/Os ions [37, 38] for which the d -shell excitations are explicitly computed. All-electron triple-zeta basis sets supplemented with two d polarization functions [39] were applied for each of the six adjacent O ligands. The eight Ba nearest neighbors were in each case modeled by Ba^{2+} ‘total-ion’ pseudopotentials (TIP’s) supplemented with a single s function [40]. For Ba_2YMoO_6 , the six nearby Y sites were described by ECP’s and valence basis functions of double-zeta quality [37]. In $\text{Ba}_2\text{LiOsO}_6$ and $\text{Ba}_2\text{NaOsO}_6$, we employed TIP’s for the six nearest Li and Na cations and sets of one s and one p functions [41]. The farther solid-state surroundings enter the quantum chemistry calculations at the level of a Madelung ionic potential. How the complexity and accuracy of quantum chemistry calculations for an infinite solid can be systematically increased is addressed in, e.g., Refs. [32, 33, 42, 43].

For the CASSCF calculations of the d -shell splittings, we used active spaces of either three (t_{2g}) or five (t_{2g} plus e_g) orbitals. The CASSCF optimizations were carried out for an average of either the ${}^2T_{2g}(t_{2g}^1)$ or ${}^2T_{2g}(t_{2g}^1) + {}^2E_{2g}(e_g^1)$ eigenfunctions of the scalar relativistic Hamiltonian. All O $2p$ and Mo/Os $4d/5d$ electrons on the reference TMO_6 octahedron were correlated in the MRCI treatment. The latter was performed with single and double substitutions with respect to the CASSCF reference, as described in Refs. [44, 45]. The spin-orbit treatment was carried out according to the procedure described in Ref. [46].

The g factors were computed following a scheme proposed by Bolvin [47] and Vancoillie [48]. For a Kramers-doublet

ground state $\{\psi, \bar{\psi}\}$, the Abragam-Bleaney tensor [11] $\mathbf{G} = gg^T$ can be expressed in matrix form as

$$\begin{aligned} G_{kl} &= 2 \sum_{u,v=\psi,\bar{\psi}} \langle u | \hat{L}_k + g_e \hat{S}_k | v \rangle \langle v | \hat{L}_l + g_e \hat{S}_l | u \rangle \\ &= \sum_{m=x,y,z} \left(A_{km} + g_e \sum_{km} \right) \left(A_{lm} + g_e \sum_{lm} \right), \end{aligned} \quad (4)$$

where g_e is the free-electron g factor and

$$\begin{aligned} A_{kx} &= 2\text{Re}[\langle \bar{\psi} | \hat{L}_k | \psi \rangle], & \sum_{kx} &= 2\text{Re}[\langle \bar{\psi} | \hat{S}_k | \psi \rangle], \\ A_{ky} &= 2\text{Im}[\langle \bar{\psi} | \hat{L}_k | \psi \rangle], & \sum_{ky} &= 2\text{Im}[\langle \bar{\psi} | \hat{S}_k | \psi \rangle], \\ A_{kz} &= 2[\langle \psi | \hat{L}_k | \psi \rangle], & \sum_{kz} &= 2[\langle \psi | \hat{S}_k | \psi \rangle]. \end{aligned} \quad (5)$$

The matrix elements of \hat{L} were extracted from the MOLPRO outputs, while the matrix elements of \hat{S} were derived using the conventional expressions for the generalized Pauli matrices:

$$\begin{aligned} (\hat{S}_z)_{MM'} &= M \delta_{MM'}, \\ (\hat{S}_x)_{MM'} &= \frac{1}{2} \sqrt{(S+M)(S-M+1)} \delta_{M-1,M'} \\ &\quad + \frac{1}{2} \sqrt{(S-M)(S+M+1)} \delta_{M+1,M'}, \\ (\hat{S}_y)_{MM'} &= -\frac{i}{2} \sqrt{(S+M)(S-M+1)} \delta_{M-1,M'} \\ &\quad + \frac{i}{2} \sqrt{(S-M)(S+M+1)} \delta_{M+1,M'}, \end{aligned} \quad (6)$$

The g factors were calculated as the positive square roots of the three eigenvalues of \mathbf{G} .

ACKNOWLEDGEMENTS

We thank V. Kataev for discussions. Part of the computations were carried out at the High Performance Computing Center (ZIH) of the Technical University Dresden. We acknowledge financial support from the German Research Foundation (Deutsche Forschungsgemeinschaft, DFG)–SFB-1143 and HO-4427/2.

COMPETING INTERESTS

The authors declare no competing financial interests.

CONTRIBUTIONS

L.X. carried out the *ab initio* quantum chemistry calculations, with assistance from N.A.B., A.P., P.F. and L.H. The mapping of the *ab initio* data onto the effective vibronic model was performed by L.X., P.F. and L.H. L.H., P.F. and J.v.d.B. designed the project. L.X. and L.H. wrote the paper, with contributions from all other coauthors.

* Correspondence: l.xu@ifw-dresden.de

† Correspondence: l.hozoi@ifw-dresden.de

- [1] Kim, B. J. *et al. Phys. Rev. Lett.* **2008**, *101*, 076402.
- [2] Witczak-Krempa, W.; Chen, G.; Kim, Y. B.; Balents, L. *Annu. Rev. Condens. Matter Phys.* **2014**, *5*, 57–82.
- [3] Jackeli, G.; Khaliullin, G. *Phys. Rev. Lett.* **2009**, *102*, 017205.
- [4] Gretarsson, H. *et al. Phys. Rev. B* **2013**, *87*, 220407.
- [5] Chun, S. H. *et al. Nat. Phys.* **2015**, *11*, 462–466.
- [6] Yamaji, Y.; Nomura, Y.; Kurita, M.; Arita, R.; Imada, M. *Phys. Rev. Lett.* **2014**, *113*, 107201.
- [7] Katukuri, V. M. *et al. New J. Phys.* **2014**, *16*, 013056.
- [8] Bogdanov, N. A. *et al. Nat. Commun.* **2015**, *6*, 7306.
- [9] Chaloupka, J.; Jackeli, G.; Khaliullin, G. *Phys. Rev. Lett.* **2010**, *105*, 027204.
- [10] Kotani, M. *J. Phys. Soc. Jap.* **1949**, *4*, 293–297.
- [11] Abragam, A.; Bleaney, B. *Electron Paramagnetic Resonance of Transition Ions*; Clarendon Press, Oxford, 1970; pp 417–426.
- [12] Mabbs, F. E.; Machin, D. J. *Magnetism and Transition Metal Complexes*; Chapman and Hall, London, 1973; pp 68–84.
- [13] Cussen, E. J.; Lynham, D. R.; Rogers, J. *Chem. Mater.* **2006**, *18*, 2855–2866.
- [14] Aharen, T. *et al. Phys. Rev. B* **2010**, *81*, 224409.
- [15] de Vries, M. A.; McLaughlin, A. C.; Bos, J.-W. G. *Phys. Rev. Lett.* **2010**, *104*, 177202.
- [16] Carlo, J. P. *et al. Phys. Rev. B* **2011**, *84*, 100404.
- [17] Qu, Z. *et al. J. Appl. Phys.* **2013**, *113*, 17E137.
- [18] Stitzer, K. E.; Smith, M. D.; zur Loye, H.-C. *Solid State Sci.* **2002**, *4*, 311–316.
- [19] Erickson, A. S. *et al. Phys. Rev. Lett.* **2007**, *99*, 016404.
- [20] Steele, A. J. *et al. Phys. Rev. B* **2011**, *84*, 144416.
- [21] Stevens, K. W. H. *On the Magnetic Properties of Covalent XY₆ Complexes*; 1953; Vol. 219; pp 542–555.
- [22] Chen, G.; Pereira, R.; Balents, L. *Phys. Rev. B* **2010**, *82*, 174440.
- [23] Gangopadhyay, S.; Pickett, W. E. *Phys. Rev. B* **2015**, *91*, 045133.
- [24] Helgaker, T.; Jørgensen, P.; Olsen, J. *Molecular Electronic-Structure Theory*; Wiley, 2000.
- [25] Faughnan, B. W. *Phys. Rev. B* **1972**, *5*, 4925–4931.
- [26] Katukuri, V. M. *et al. Inorg. Chem.* **2014**, *53*, 4833–4839.
- [27] Wiebe, C. R. *et al. Phys. Rev. B* **2003**, *68*, 134410.
- [28] McLaughlin, A. C. *Phys. Rev. B* **2008**, *78*, 132404.
- [29] Wallace, T. K.; Colman, R. H.; McLaughlin, A. C. *Phys. Chem. Chem. Phys.* **2013**, *15*, 8672–8677.
- [30] Kahn, O.; Kettle, S. F. A. *Mol. Phys.* **1975**, *29*, 61–79.
- [31] Prosandeev, S. A.; Waghmare, U.; Levin, I.; Maslar, J. *Phys. Rev. B* **2005**, *71*, 214307.
- [32] Doll, K.; Dolg, M.; Fulde, P.; Stoll, H. *Phys. Rev. B* **1997**, *55*, 10282–10288.
- [33] Yang, J. *et al. Science* **2014**, *345*, 640–643.
- [34] Hozoi, L. *et al. Phys. Rev. B* **2014**, *89*, 115111.
- [35] Bogdanov, N. A. *et al. Phys. Rev. Lett.* **2013**, *110*, 127206.
- [36] Werner, H. J.; Knowles, P. J.; Knizia, G.; Manby, F. R.; Schütz, M. *Wiley Rev: Comp. Mol. Sci.* **2012**, *2*, 242–253.
- [37] Peterson, K. A.; Figgen, D.; Dolg, M.; Stoll, H. *J. Chem. Phys.* **2007**, *126*, 124101.
- [38] Figgen, D.; Peterson, K. A.; Dolg, M.; Stoll, H. *J. Chem. Phys.* **2009**, *130*, 164108.
- [39] Dunning, T. H. *J. Chem. Phys.* **1989**, *90*, 1007–1023.
- [40] Lim, I. S.; Stoll, H.; Schwerdtfeger, P. *J. Chem. Phys.* **2006**, *124*, 034107.
- [41] Fuentealba, P.; Preuss, H.; Stoll, H.; von Szentpály, L. *Chem. Phys. Lett.* **1982**, *89*, 418–422.
- [42] Fulde, P. *Nat. Phys.* **2016**, *12*, 106–107.
- [43] Fulde, P. *Correlated Electrons in Quantum Matter*; World Scientific, Singapore, 2012.
- [44] Knowles, P. J.; Werner, H.-J. *Theor. Chim. Acta* **1992**, *84*, 95–103.
- [45] Werner, H.-J.; Knowles, P. J. *J. Chem. Phys.* **1988**, *89*, 5803–5814.
- [46] Berning, A.; Schweizer, M.; Werner, H.-J.; Knowles, P. J.; Palmieri, P. *Mol. Phys.* **2000**, *98*, 1823–1833.
- [47] Bolvin, H. *ChemPhysChem* **2006**, *7*, 1575–1589.
- [48] Vancoillie, S.; Malmqvist, P.; Pierloot, K. *ChemPhysChem* **2007**, *8*, 1803–1815.